

OAK RIDGE NATIONAL LABORATORY LIBRARIES



3 4456 0569803 7

ORNL/TM-8444

ornl

**OAK
RIDGE
NATIONAL
LABORATORY**

**UNION
CARBIDE**

Unified Creep-Plasticity Constitutive Equations for 2-1/4 Cr-1 Mo Steel at Elevated Temperature

D. N. Robinson R. W. Swindeman

OAK RIDGE NATIONAL LABORATORY
CENTRAL RESEARCH LIBRARY
CIRCULATION SECTION
4500N ROOM 175

LIBRARY LOAN COPY

DO NOT TRANSFER TO ANOTHER PERSON.
If you wish someone else to see this report, send in
name with report and the library will arrange a loan.

ORNL-118 (6-97)

**OPERATED BY
UNION CARBIDE CORPORATION
FOR THE UNITED STATES
DEPARTMENT OF ENERGY**



Printed in the United States of America. Available from
the U.S. Department of Energy
Technical Information Center
P.O. Box 62, Oak Ridge, Tennessee 37830

This report was prepared as an account of work sponsored by an agency of the United States Government. Neither the United States Government nor any agency thereof, nor any of their employees, makes any warranty, express or implied, or assumes any legal liability or responsibility for the accuracy, completeness, or usefulness of any information, apparatus, product, or process disclosed, or represents that its use would not infringe privately owned rights. Reference herein to any specific commercial product, process, or service by trade name, trademark, manufacturer, or otherwise, does not necessarily constitute or imply its endorsement, recommendation, or favoring by the United States Government or any agency thereof. The views and opinions of authors expressed herein do not necessarily state or reflect those of the United States Government or any agency thereof.



ORNL/TM-8444
Dist. Category UC-79T, -79Th,
-79Tk
OR-1.1, High-Temperature
Structural Design Technology

Contract No. W-7405-eng-26

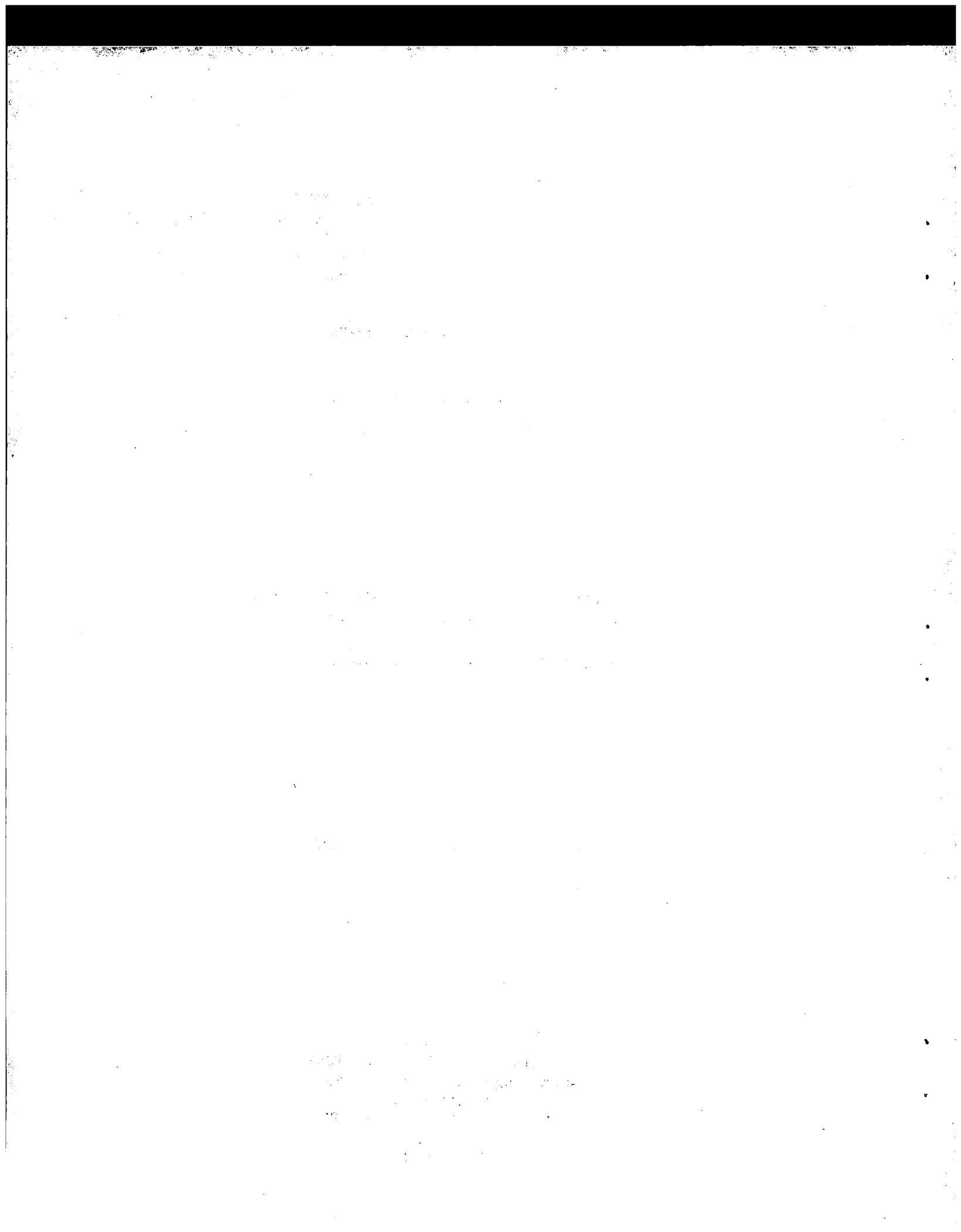
Engineering Technology Division

UNIFIED CREEP-PLASTICITY CONSTITUTIVE EQUATIONS FOR
2-1/4 Cr-1 Mo STEEL AT ELEVATED TEMPERATURE

D. N. Robinson R. W. Swindeman

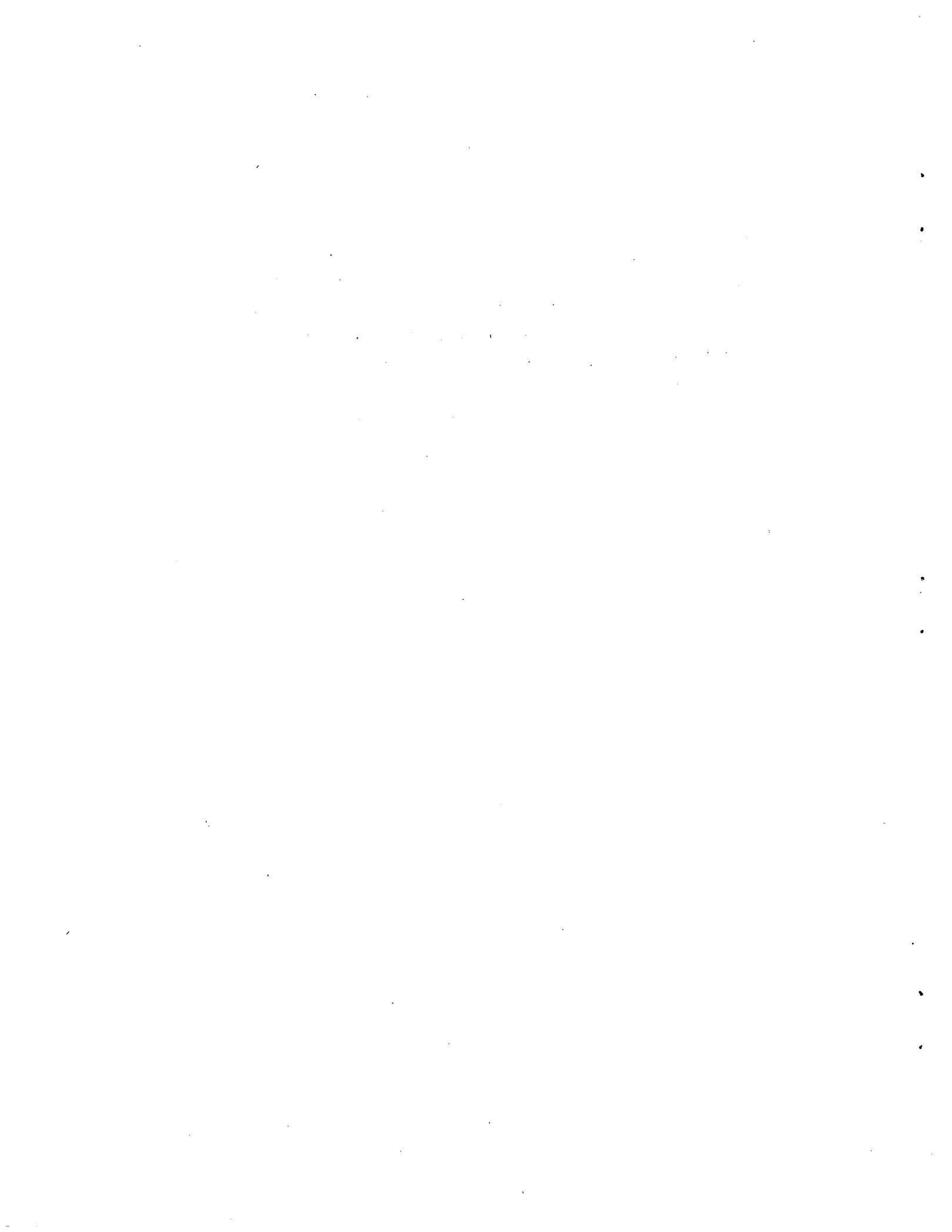
Date Published - October 1982

Prepared by
OAK RIDGE NATIONAL LABORATORY
Oak Ridge, Tennessee 37830
operated by
UNION CARBIDE CORPORATION
for the
DEPARTMENT OF ENERGY



CONTENTS

	<u>Page</u>
ABSTRACT	1
1. INTRODUCTION	1
2. THE UNIFIED EQUATIONS FOR 2-1/4 Cr-1 Mo STEEL (PWHT)	4
3. CALCULATED RESULTS USING THE UNIFIED EQUATIONS	8
4. GENERAL PROPERTIES OF SOLUTIONS USING THE UNIFIED EQUATIONS	21
5. SUMMARY AND CONCLUSIONS	30
ACKNOWLEDGMENTS	32
REFERENCES	33



UNIFIED CREEP-PLASTICITY CONSTITUTIVE EQUATIONS FOR
2-1/4 Cr-1 Mo STEEL AT ELEVATED TEMPERATURE*

D. N. Robinson R. W. Swindeman

ABSTRACT

Unified creep/plasticity constitutive equations are provided for 2-1/4 Cr-1 Mo steel in a post-weld heat-treated condition. These equations are recommended for trial use in inelastic design analyses for breeder reactor components at high temperature. The range of applicability of the equations is approximately 250 to 600°C in temperature and strain rates not in excess of about 0.04/min. The model is multiaxial and nonisothermal and accounts for both rate-dependent plasticity and creep. The results of several calculations based on the unified equations are included to provide a test of the correct implementation of the model and to demonstrate the predictive capability of the model. Also, a discussion is included regarding general properties of solutions to structural problems when employing the unified equations.

Keywords: viscoplasticity, constitutive equations, high-temperature plasticity, creep, structural analysis, rate sensitivity, time dependency.

1. INTRODUCTION

The purpose of this report is to document for trial use the Oak Ridge National Laboratory (ORNL) unified equations for the liquid-metal fast breeder reactor (LMFBR) steam generator material 2-1/4 Cr-1 Mo steel. The model parameters have been determined to represent the elevated-temperature behavior of a vacuum arc remelted (VAR) heat of 2-1/4 Cr-1 Mo steel (heat 56448) in a 40-h post-weld heat-treated (PWHT) condition. An exact specification of the material composition and heat treatment, as well as the results of numerous characterization tests, are found in

*Work performed under DOE/OBTP AF 15 40 10 3, Task No. OR-1.1, High-Temperature Structural Design Technology.

Refs. 1 and 2. The chosen heat and post-weld heat treatment are prototypical of the LMFBR steam generator material and conditions.

As the present data base is largely exploratory and thus somewhat limited, the range of applicability of the model as specified here is limited to about 250 (482) to 600°C (1112°F) in temperature and strain rates below about 0.04/min. This range includes most important thermal transients relating to LMFBR steam generator design.

A complete multiaxial and nonisothermal specification of the constitutive model is presented with numerical values for each of the material parameters. As previously discussed,³ the ORNL unified equations are of the Bailey-Orowan type and make use of the earlier experimental and theoretical work of several authors including Rice,⁴ Ponter and Leckie,⁵ Mitra and McLean,⁶ Lagneborg,⁷ and Onat.⁸ The relationship with those works has been discussed at length³ and will not be repeated here.

As the unified model admits analytically different mathematical descriptions in various regions of the state space,^{3,8} guidance is provided for numerically smoothing across the boundaries of these regions. The smoothing procedure described herein is intended primarily as an example; it was used with satisfactory results in implementing the unified equations in the ORNL finite element code PLACRE by W. K. Sartory of ORNL.

The results of several calculations are given for two reasons — first, to provide a convenient check on the correct implementation of the unified equations in a structural analysis code, and, second, to furnish further comparisons with experimental data to demonstrate the accuracy of the model in representing both rate-dependent plasticity, on the one hand, and creep behavior on the other. Included in these calculations is a two-bar ratchetting problem. For comparison, the results of the corresponding two-bar experiment have been presented in Ref. 9 and in an appendix of NE standard F 9-5T¹⁰ where they are used as verification of the F 9-5T α -reset option for 2-1/4 Cr-1 Mo steel. The α -reset option introduced in F 9-5T is but a time-independent specialization of the time-dependent recovery mechanisms built into the unified equations.

Also presented are solutions to two prototypical structural problems, one illustrating the redistribution of stress during creep of a thick-walled cylinder under constant internal pressure and the second involving the (nonradial) response of a cylinder subjected to a thermal shock.

Finally, a discussion is given of the general properties of solutions of structural problems when employing the ORNL unified constitutive equations. Such questions as the sensitivity of solutions to the prescribed initial stress and state fields, uniqueness of solution, and shakedown are discussed.

2. THE UNIFIED EQUATIONS FOR 2-1/4 Cr-1 Mo STEEL (PWHT)

The constitutive equations recommended in NE standard F 9-5T¹⁰ for 2-1/4 Cr-1 Mo steel are classically based and rest on the assumption that the inelastic strain can be decomposed into two additive contributions, one time independent (plasticity) and one time dependent (creep). Experimental evidence does not generally support this assumption, however, and suggests representations in which creep and plasticity are characterized as occurring simultaneously and interactively (unified). The constitutive equations presented in this section are unified in that sense.

A complete statement of the unified equations for VAR heat 56448 of 2-1/4 Cr-1 Mo steel is as follows.*

$$2\bar{\mu}\dot{\epsilon}_{ij} = \begin{cases} F^n \frac{\Sigma_{ij}}{\sqrt{J_2}} ; & F > 0 \text{ and } S_{ij}\Sigma_{ij} > 0 \\ 0 & ; F \leq 0 \text{ or } F > 0 \text{ and } S_{ij}\Sigma_{ij} \leq 0 \end{cases} , \quad (2.1)$$

$$\dot{\alpha}_{ij} = \begin{cases} 2\mu h \dot{\epsilon}_{ij} - r \frac{\alpha_{ij}}{\sqrt{I_2}} ; & G > G_0 \text{ and } S_{ij}\alpha_{ij} > 0 \\ 2\mu h_0 \dot{\epsilon}_{ij} - r_0 \frac{\alpha_{ij}}{\sqrt{I_2}} ; & G \leq G_0 \text{ or } S_{ij}\alpha_{ij} \leq 0 \end{cases} , \quad (2.2)$$

where

$$F = (J_2/\kappa^2) - 1 , \quad (2.3)$$

$$G = \sqrt{I_2/\kappa^2} , \quad (2.4)$$

$$J_2 = \frac{1}{2} \Sigma_{ij}\Sigma_{ij} , \quad (2.5)$$

$$I_2 = \frac{1}{2} \alpha_{ij}\alpha_{ij} , \quad (2.6)$$

*Following the usual Cartesian tensor notation, repeated subscripts imply summation.

$$h = \frac{H}{G^\beta} ; h_o = \frac{H}{G_o^\beta} , \quad (2.7)$$

$$r = RG^{m-\beta} ; r_o = RG_o^{m-\beta} . \quad (2.8)$$

Here, $\dot{\epsilon}_{ij}$ denotes the inelastic strain rate, Σ_{ij} the effective stress (i.e., $\Sigma_{ij} = S_{ij} - \alpha_{ij}$), and S_{ij} the deviatoric stress.*

The state variables are α_{ij} and κ ; however, the scalar threshold (Bingham) stress, κ , is taken to be constant $\kappa = 0.82 \text{ ksi}^\dagger$ because of the almost total absence of isotropic hardening in this alloy in the PWHT condition.²

All of the characterization testing was conducted on the isotropically saturated material, which was obtained by cycling over four to five cycles at the test temperature.^{1,2} Numerical values for the parameters appearing in Eqs. (2.1) through (2.8) are:

$$\begin{aligned} \mu &= 3.61 \times 10^7 ; \bar{\mu} = \mu \exp(-\theta_1) , \dots \dots (h) \\ n &= 4 , \\ m &= 7.73 , \\ \beta &= 1.5 , \\ R &= 9.0 \times 10^{-3} \exp(\theta_2) , \dots \dots \dots (ksi/h) \\ H &= 1.37 \times 10^{-4} , \dots \dots \dots (ksi/h) \\ G_o &= 0.14 , \end{aligned}$$

with

$$\theta_1 = (23.8 \theta - 2635) (1/811 - 1/\theta) , \quad (2.9)$$

$$\theta_2 = 40,000 (1/811 - 1/\theta) . \quad (2.10)$$

Here, θ is the absolute temperature in Kelvin (K).[†] As noted, the other parameter values are consistent with physical units of ksi^\dagger for stress and h for time.

*This formulation is given in the context of infinitesimal strain. In the case of finite strain, the equations should be interpreted as relating the Euler rate-of-deformation tensor to the Cauchy stress.¹¹

[†] 6.895 MPa = 1 ksi.

[‡] °F = 9/5 (K - 273) + 32.

The inequalities in Eqs. (2.1) through (2.8) define boundaries across which the flow [Eq. (2.1)] and evolutionary [Eq. (2.2)] equations change form discontinuously. Although the inelastic strain ϵ_{ij} and the state variable α_{ij} remain continuous, their rates of change are idealized as having possible discontinuities. This permits modeling of observed phenomena such as hesitation periods in creep (or stress relaxation) following partial stress reductions and the rapid readjustment of internal state (dynamic recovery) that accompanies remobilization of dislocations under reversed stressing. The latter has a direct bearing on the correct modeling of cyclic response that is so important in breeder reactor applications. Of course, there is strong precedent in applied mechanics for idealizing boundaries of rapid change as analytic discontinuities, e.g., as in classical plasticity.

For numerical purposes the discontinuous state boundaries can be smoothed as follows. A smooth spline function $P(x)$ is first defined on $(-1,1)$ according to*

$$P(x) = (1 + x)^2/2 \quad ; \quad -1 \leq x \leq 0 \quad (2.11)$$

$$P(x) = 1 - (1 - x)^2/2 \quad ; \quad 0 \leq x \leq 1 \quad (2.12)$$

$$P(x) = 0 \quad ; \quad x < -1 \quad (2.13)$$

$$P(x) = 1 \quad ; \quad x > 1 \quad (2.14)$$

The function F in Eqs. (2.3) and (2.1) can then be replaced by F defined by:

$$F = P\left(\frac{S_{ij} \cdot \Sigma_{ij}}{W_1}\right) \langle F \rangle \quad , \quad (2.15)$$

where W_1 is a smoothing width selected by the analyst and the angular brackets denote

$$\langle x \rangle = x \quad ; \quad x \geq 0 \quad (2.16)$$

*Note that smoothness can be carried to higher derivatives if necessary.

and

$$\langle x \rangle = 0 ; x < 0 . \quad (2.17)$$

The use of Eq. (2.15) appropriately smoothes the discontinuity in $\dot{\epsilon}_{ij}$ across $S_{ij} \Sigma_{ij} = 0$ and, as well, eliminates each of the inequalities appearing in the flow law, Eq. (2.1).

The discontinuous nature of $\dot{\alpha}_{ij}$ in Eq. (2.2) can be smoothed by first replacing the sharp G cutoff by a gradual one, e.g.,

$$G' = \begin{cases} G & ; G \geq 2G_0 \\ \frac{G^2}{4G_0} + G_0 & ; G < 2G_0 \end{cases} \quad (2.18)$$

$$(2.19)$$

and then calling

$$G = (G' - G_0) P \left(\frac{S_{ij} \alpha_{ij}}{W_2} \right) + G_0 . \quad (2.20)$$

Equations (2.7) and (2.8) may then be written

$$h = h_0 = \frac{H}{G^\beta} \quad (2.21)$$

and

$$r = r_0 = R G^{m-\beta} , \quad (2.22)$$

so that the evolutionary law, Eq. (2.2), reduces to a single expression providing a smooth transition across $S_{ij} \alpha_{ij} = 0$ in the state space and, once again, no inequalities.

As before, W_2 is a smoothing width chosen by the user. Values for W_1 and W_2 used in the finite element code PLACRE in conducting most of the analyses reported in the following section were

$$W_1 = W_2 = 10^{-2} \text{ (ksi}^2\text{)} = 0.475 \text{ (MPa}^2\text{)} .$$

3. CALCULATED RESULTS USING THE UNIFIED EQUATIONS

Several calculations based on the foregoing constitutive relations have been made and their results are included in this section. It is suggested that at least some of these results be reproduced to verify the correct implementation of the constitutive model into a given analysis code. Comparative experimental results are shown with some of the calculated results as a measure of the predictive accuracy of the model.

Figure 1 shows predictions (solid lines) of stable hysteretic loops generated over a strain range of approximately $\pm 0.32\%$ at strain rates of 0.04, 0.004, and 0.0004/min and at 538°C (1000°F). Also shown is a sampling of experimental data for the same conditions and spanning the range of strain rates. The model is seen to capture the viscoplastic strain-rate dependence at the reference temperature 538°C (1000°F) very well. This is not unexpected as data of this type were used as part of the data base in characterizing strain-rate dependency.^{1,2,12}

The strain rate 0.004/min is considered *fast* in LMFBR technology. The model, as characterized here, thus allows for an order of magnitude above that strain rate.

A comparison of predicted and observed creep-time curves corresponding to a stress range of about 55-103 MPa (8-15 ksi) and a temperature of 538°C (1000°F) is shown in Fig. 2. The creep curves show a relatively short transient creep period followed by *steady-state* creep. The predictions generally show higher initial creep rates in the transient period; however, these are known to be strongly dependent on the loading ramp rate. This was not known precisely in the experiments. The loading ramp rate in the predictions was taken as 0.06%/h.

Measured and predicted secondary creep rate and total creep strain compare very well in Fig. 2. Once again, regarding the secondary creep rate, good agreement is to be expected in as much as *steady-state* creep data were included as part of the characterization data base.¹² It is, of course, essential that steady-state creep rates be represented accurately in constitutive equations for LMFBR applications. Additional evidence demonstrating the appropriate modeling of secondary creep rates

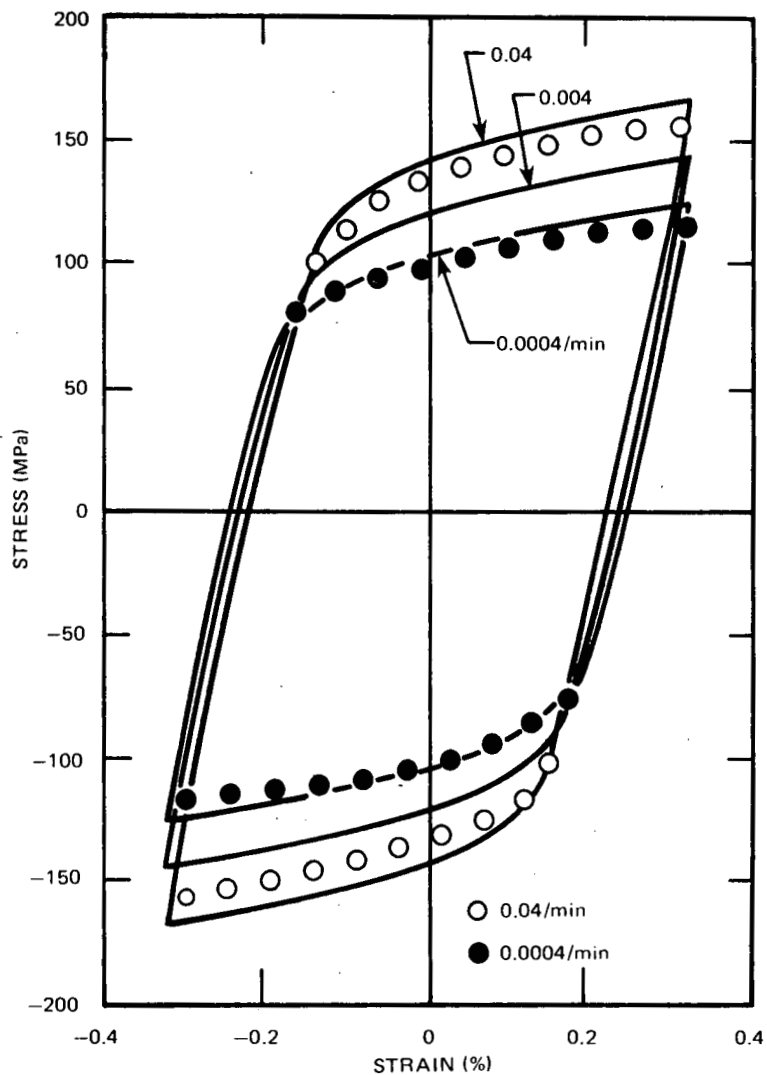


Fig. 1. Modeled (solid lines) and experimental (dots) stable hysteresis loops for $\Delta\epsilon \approx \pm 0.32\%$ at various strain rates. The temperature is 538°C (1000°F). ($6.895\text{ MPa} = 1\text{ ksi}$)

at both the reference temperature 538°C (1000°F) and at 510°C (950°F) is shown in Fig. 3.

Because most critical structural problems related to the design of LMFBR components are nonisothermal, it is necessary that the thermo-mechanical behavior of the structural alloys of interest be appropriately modeled. To this end, both isothermal tests at several fixed temperatures — such as those referred to earlier in the case of secondary creep —

ORNL-DWG 82-6229 ETD

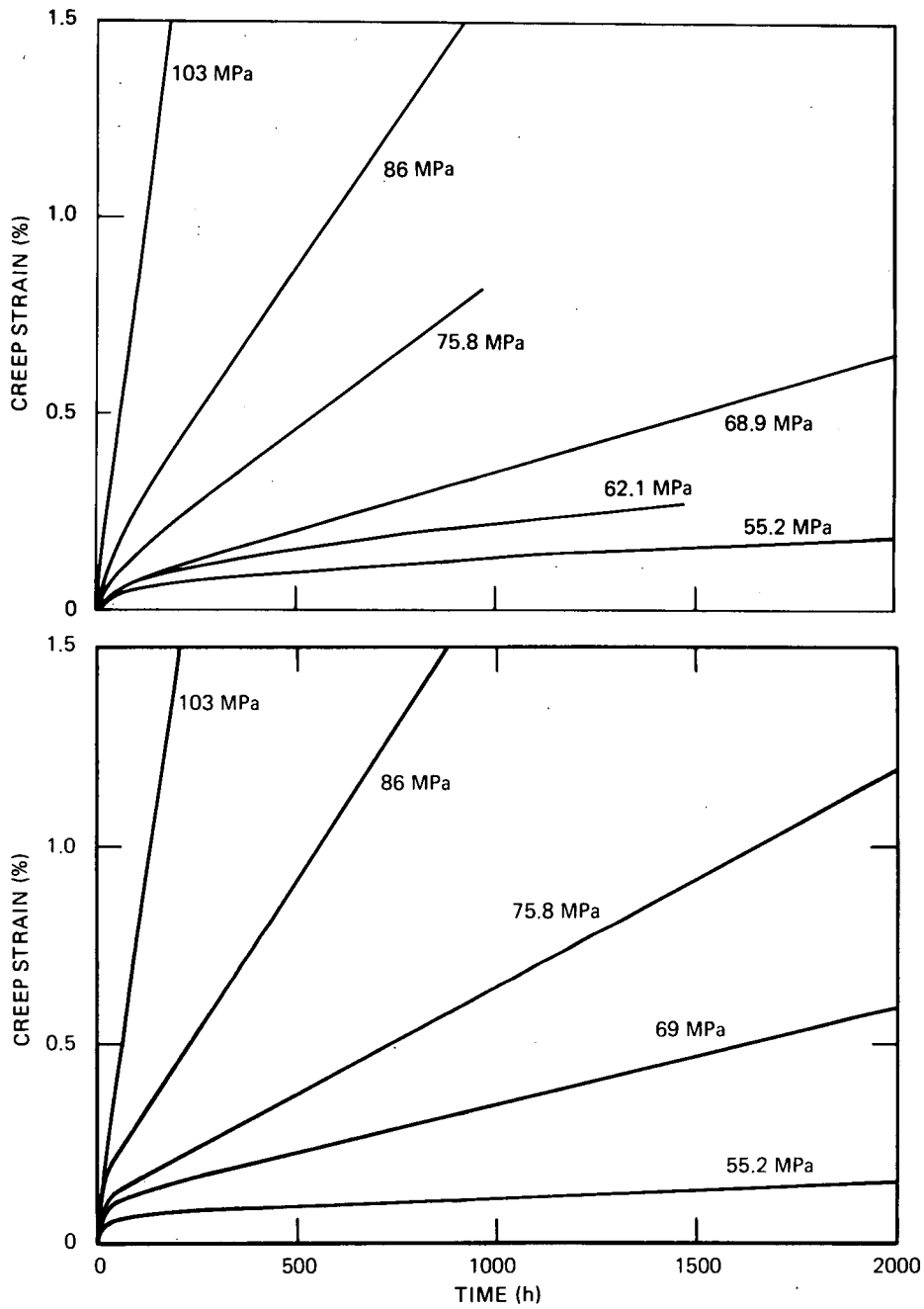


Fig. 2. Modeled (lower figure) and experimental (upper figure) creep-time curves for the indicated stress levels at 538°C (1000°F). (6.895 MPa = 1 ksi)

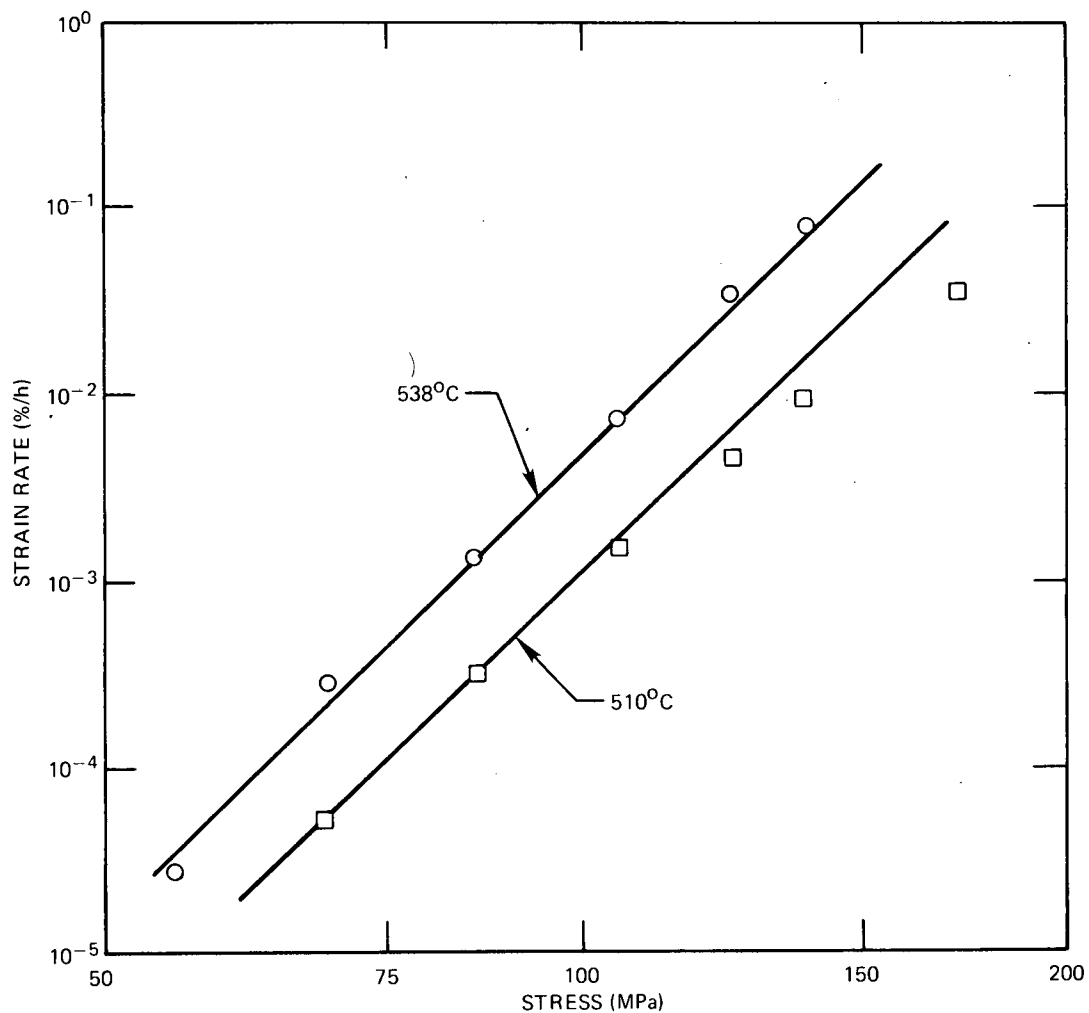


Fig. 3. Steady-state creep rate vs stress at 538°C (1000°F) and 510°C (950°F). Solid lines, modeled; dots, experimental. (6.895 MPa = 1 ksi)

and truly nonisothermal tests have been included as part of the data base for the unified equations. An example of the type of nonisothermal experiment used is shown in Fig. 4. Here, a uniaxial specimen initially at 811 K (538°C - 1000°F) and zero stress is constrained axially; the temperature is then cycled at a rate of 50°C/min (90°F/min) between the initial temperature 811 K (538°C - 1000°F) and 573 K (300°C - 572°F). This cycle causes appreciable yielding and gives rise to the stable hysteretic loop indicated by the dots in Fig. 4; the solid line represents the predicted response. Data of this type were included in the selection

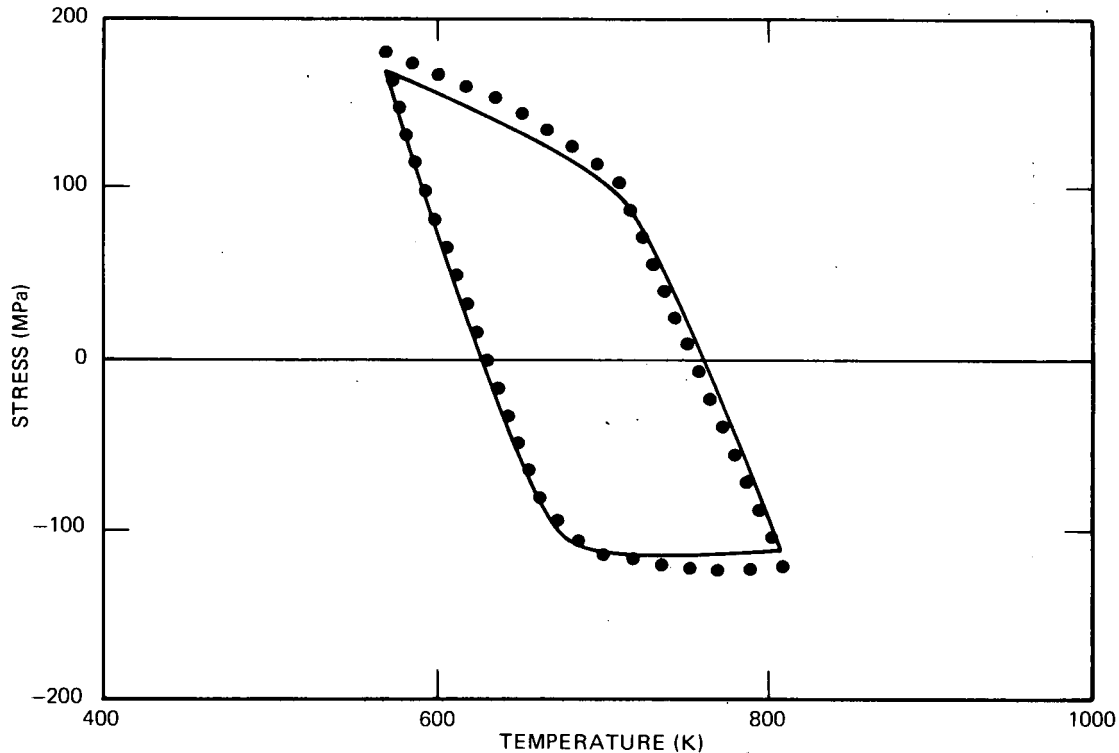


Fig. 4. Predicted (solid line) and measured (dots) response for nonisothermal test conducted between 811 K (538°C) and 573 K (300°C) at $\sim 50^\circ\text{C}/\text{min}$. (6.895 MPa = 1 ksi)

of the material parameters in the Arrhenius forms of Eqs. (2.9) and (2.10). The prediction of this test is quite satisfactory and provides a useful result for checking the proper implementation of the nonisothermal aspects of the unified model.

Figure 5 shows the predicted redistribution of hoop (circumferential) stress with time in an internally pressurized cylinder. The cylinder dimensions are prototypical of LMFBR steam generator tubes, having an inner radius of 4.06 mm (0.16 in.) and an outer radius of 6.35 mm (0.25 in.). The loading history consists of a 10 s ramp up to an internal pressurization of 25.17 MPa (3.65 ksi) followed by a hold period at that pressure. The temperature is constant at 566°C (1050°F). Figure 5 shows the predicted distribution of hoop stress at several times following pressurization (zero time denotes the end of the loading ramp). The

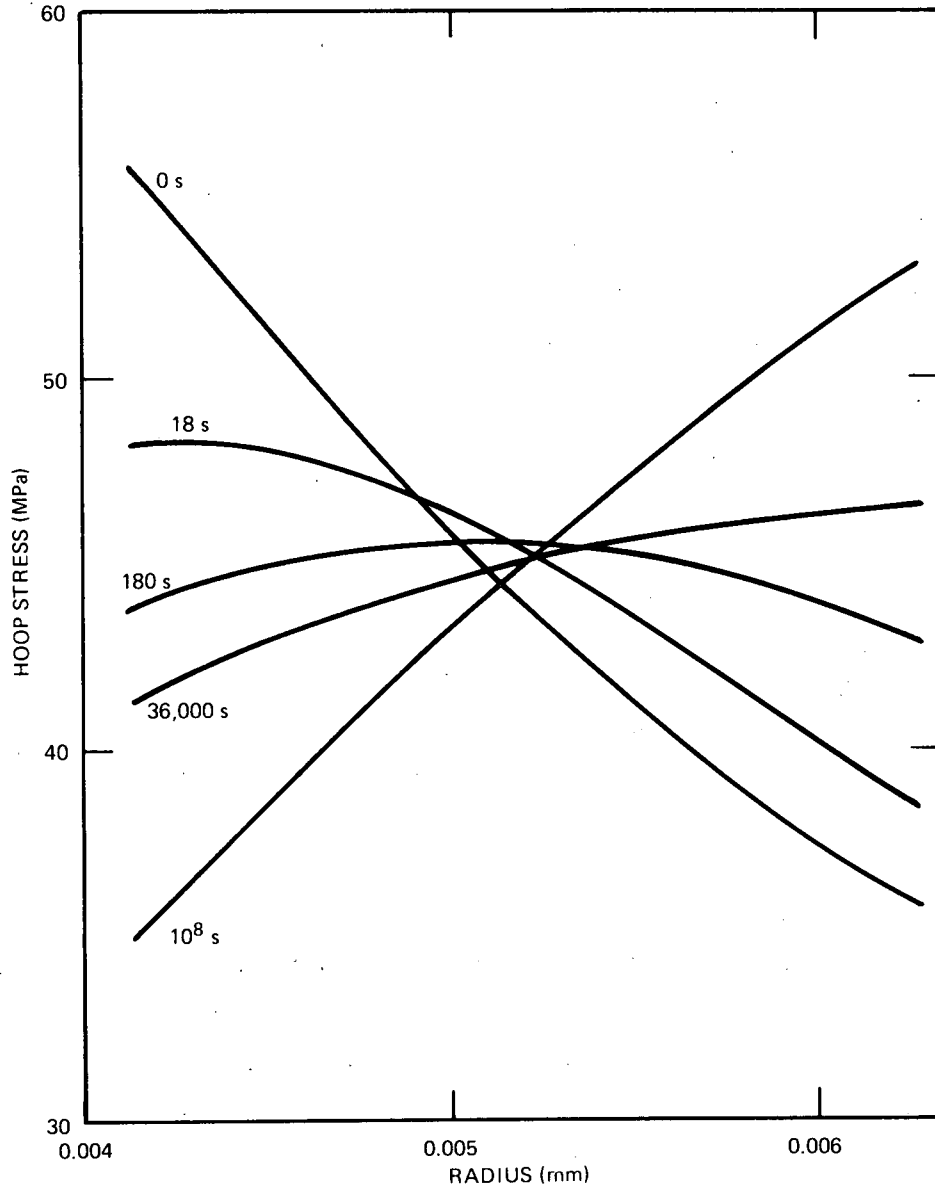


Fig. 5. Predicted redistribution of hoop (circumferential) stress with time in a cylinder under constant internal pressurization. Inner radius = 4.06 mm (0.16 in.), outer radius = 6.35 mm (0.20 in.), and pressure = 25.17 MPa (3.65 ksi). (6.895 MPa = 1 ksi)

behavior appears typical, exhibiting an initially rapid redistribution* of stress followed finally by a stress distribution essentially constant in time (e.g., that labelled 10^8 s). Note that a *reference stress* of about 45 MPa (6.5 ksi) is indicated at a radius of roughly 5.2 mm (0.20 in.).

Despite the apparent simplicity of the problem depicted in Fig. 5, it is one that exemplifies the potential numerical *stiffness* of this class of constitutive equations. The simultaneous presence of a relatively fast transient and a slowly varying steady-state-like response can, with some governing equations and under some integration schemes, lead to serious numerical instabilities and/or require extended use of very small (and costly) integration step sizes. No such difficulties were encountered here nor was a special stiff integrator used.

The most common structural problem associated with LMFBR steam generator design that necessitates detailed inelastic analysis is that of a cylinder (pipe) under inhomogeneous thermal transient loading. Such problems arise in connection with potential reactor scrams and other abnormal shutdowns. A good experimental approximation to the behavior in such situations — including creep-enhanced ratchetting — and one in which the stresses and strains are directly measurable, is the two-bar ratchetting test. A series of two-bar tests^{9,10} were conducted using 2-1/4 Cr-1 Mo steel (PWHT) under a variety of thermal shock conditions. In these tests, two uniaxial specimens are tested simultaneously in two servocontrolled electrohydraulic machines which are linked together in such a way that the sum of the loads in both bars is held constant (maintaining equilibrium), while the extension of the two bars is kept the same (maintaining compatibility). Initially, an equal axial stress is applied to both bars. Then, the temperature in bar 1 is ramped downward from the maximum temperature, T_{\max} , to a minimum, T_{\min} . Subsequently, the temperature in bar 2 is ramped downward while the temperature in bar 1 is kept at T_{\min} . After bar 2 reaches the minimum temperature, both bars are heated together to T_{\max} . The temperature is then held

*The initial rate of stress redistribution depends strongly on the loading time. Following a less rapid load up the initial redistribution would likewise be less rapid.

constant at T_{\max} for a prescribed time interval and the sequence is repeated. The response of the two bars roughly simulates the behavior of material elements at the inner and outer radii of a cylinder (pipe) under analogous conditions.

One of these tests (test A1 in Ref. 9) is included in Appendix A of Ref. 10 as evidence to substantiate the use of the α -reset option in thermal transient analyses involving this alloy, and furthermore, to demonstrate the qualitatively incorrect predictions made by the constitutive equations of Sect. 4 of Ref. 10 in the absence of the α -reset procedure. A prediction of that test using the unified equations is given here, and the results are shown in Figs. 6 and 7. The conditions of the test are $T_{\max} = 538^{\circ}\text{C}$ (1000°F), $T_{\min} = 300^{\circ}\text{C}$ (527°F), the initial stress

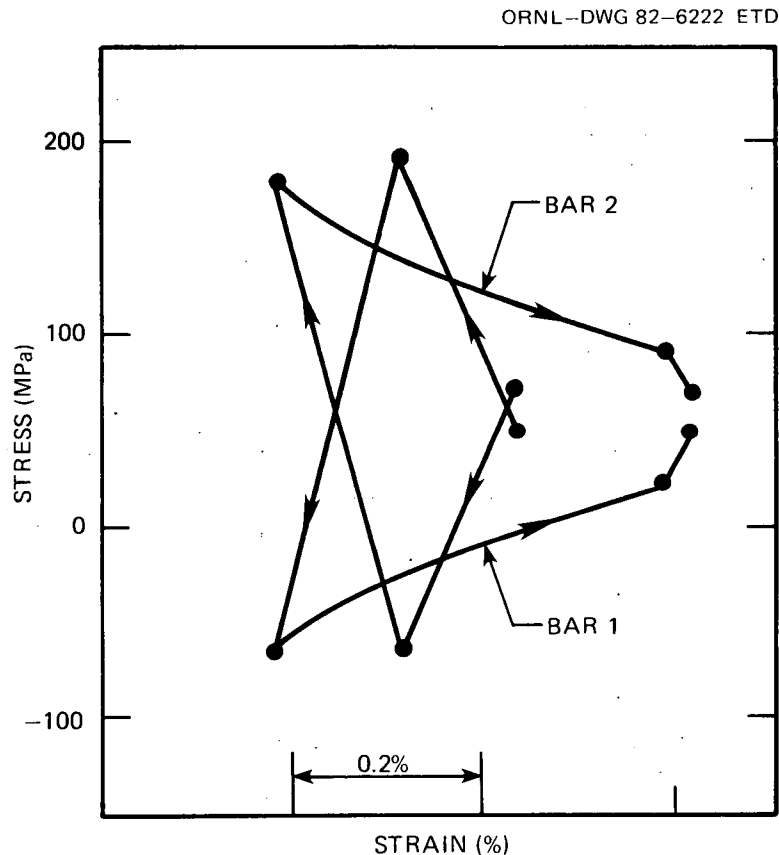


Fig. 6. Predicted stable stress-(total) strain ratchetting cycle for two-bar test A1 in Refs. 9 and 10. (6.895 MPa = 1 ksi)

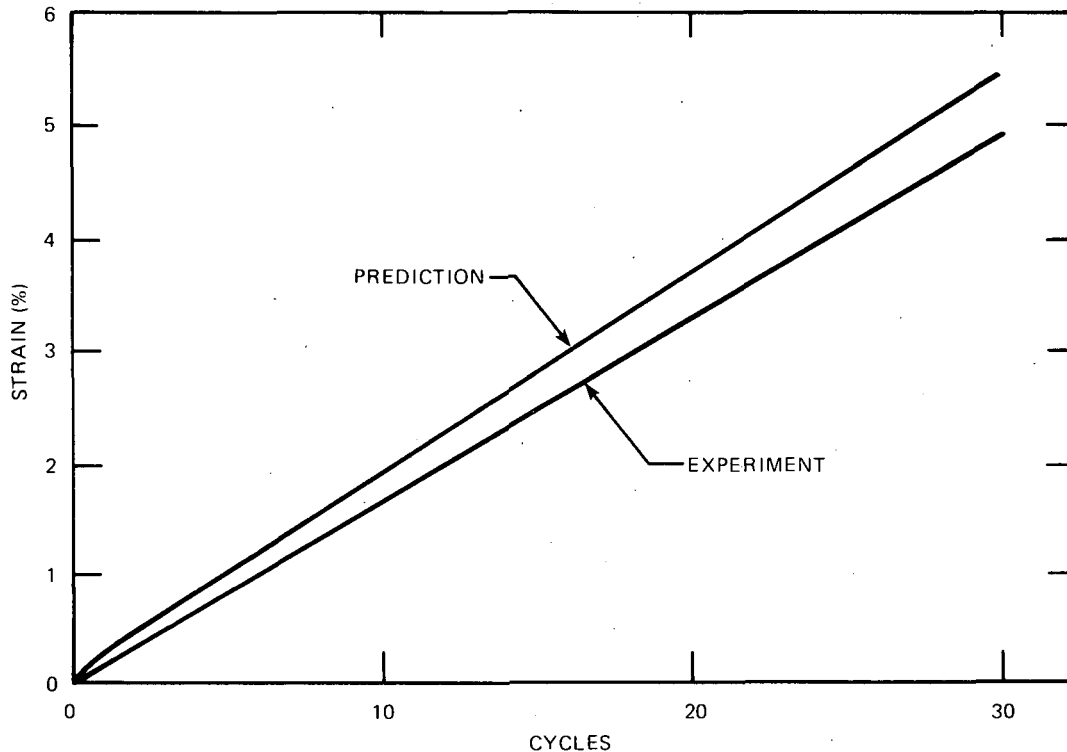


Fig. 7. Predicted and experimental ratchetting strain vs cycles for two-bar test A1 of Refs. 9 and 10.

is 58.6 MPa (8.5 ksi), the temperature ramp time is 10 min in each case, and the hold time at T_{\max} is 11.5 h.

Figure 6 shows the predicted stress-(total) strain response for each of the bars over one complete cycle. The cycle shown is typical of all cycles after about the first three, during which there is a small amount of transient adjustment. The stress peaks and the general shape of the stress-strain response in Fig. 6 compare favorably with the experimental results of Ref. 9. A key feature of the predicted results is that the peak stresses and the ratchetting strain per cycle remain essentially constant. Figure 7 shows the ratchetting strain vs cycles for the calculation and the experiment; both show a basically constant ratchetting rate and quite good agreement. The prediction just slightly overestimates the ratchetting strain.

In contrast to the features of Figs. 6 and 7, calculations made using the kinematic hardening model of Ref. 10 without the α -reset option are

qualitatively different and invariably predict saturation of ratchetting after a few cycles, thus substantially underestimating the ratchetting strain.¹³ The unified equations predict the correct qualitative response with good accuracy and without the ad hoc α -reset option. As indicated earlier, the α -reset procedure is but a time-independent idealization of the recovery mechanisms inherent in the unified theory.

The final calculation is that of a pipe under thermal ratchetting conditions. This calculation was made in connection with the design of the eighth in a series of pipe thermal ratchetting and creep-fatigue failure tests (TT-8) and aimed at assessing design analysis methods and failure criteria. The TT-8 test is proposed for testing in the Thermal Transient Facility at the Energy Technology Engineering Center. The *a priori* prediction given here will provide an excellent check* on the unified equations upon completion of the experiment.

The dimensions of the TT-8 pipe are 12.7 mm (0.50 in.) in wall thickness and a 178-mm (7-in.) inside diameter. The assumed conditions are generalized plane strain and uncoupled thermomechanical behavior. Thermal and mechanical properties for 2-1/4 Cr-1 Mo steel other than those inherent in the constitutive equations were taken from the *Nuclear Systems Materials Handbook*.¹⁴

The mechanical loading conditions for TT-8 are an axial end load of 0.60 MN (135,000 lb) with zero internal pressure. The outer surface of the pipe is taken to be ideally thermally insulated. The cyclic thermal shock history at the inside pipe surface is as follows: from a uniform maximum temperature $T_{\max} = 538^{\circ}\text{C}$ (1000°F), the inner surface is rapidly cooled at a rate of 33°C/s (60°F/s) to a temperature $T_{\min} = 260^{\circ}\text{C}$ (500°F); it is then reheated at 56°C/h (100°F/h) back to the hold temperature of 538°C (1000°F) for a 16-h hold period, completing the cycle. This represents a severe thermal transient loading condition that will be repeated to failure in the TT-8 test. The stress path (in circumferential vs axial stress space) followed by elements at both the inner and

*Comparison of predicted and measured ratchetting rate provides a valid check on the unified constitutive equations. Comparison of predicted and actual cycles to failure involves uncertain failure criteria and should not be used as a direct assessment of the unified equations.

outer surfaces is nonradial, providing a good test of the constitutive equations and analysis procedures.

Figures 8 and 9 show the predicted axial stress-strain behavior at the extreme inner and outer elements of the pipe, respectively. *Shakedown* to a repetitive hysteric loop occurs after only three or four cycles, with the peak stresses remaining constant thereafter. The magnitudes of the stress peaks are critical in the determination of creep damage using the ASME recommended damage accumulation rule of linear time-fractions. Unfortunately, stress measurements are not possible in the pipe wall, as they are in the two-bar tests discussed earlier, and cannot be compared with predictions. The only directly comparable feature is the strain at the outer surface of the pipe. Figure 10 shows the predicted axial strain at the outer surface against time. Again, a transient response of three or four cycles is evident, after which the ratchetting rate becomes essentially constant at about 0.02%/cycle.

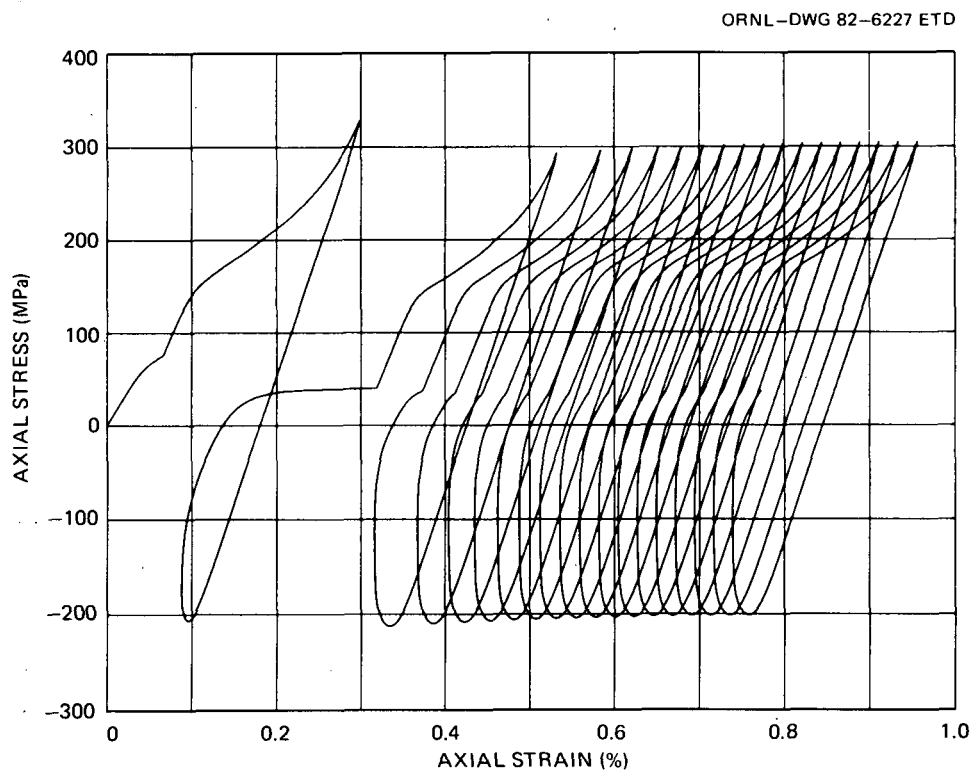


Fig. 8. Predicted axial stress vs axial strain for inner pipe element of TT-8 experiment. (6.895 MPa = 1 ksi)

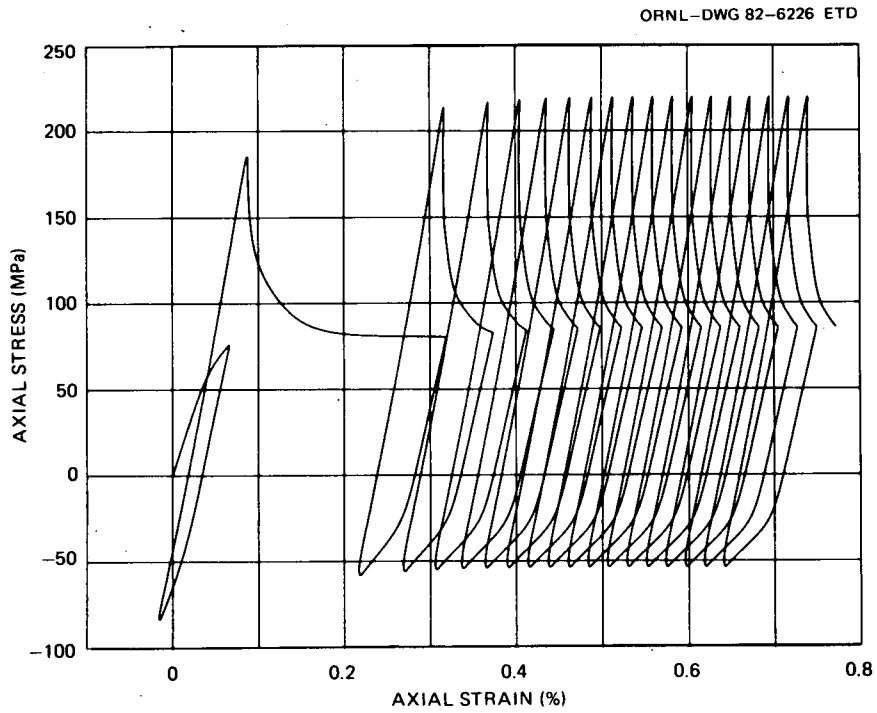


Fig. 9. Predicted axial stress vs axial strain for outer pipe element of TT-8 experiment. (6.895 MPa = 1 ksi)

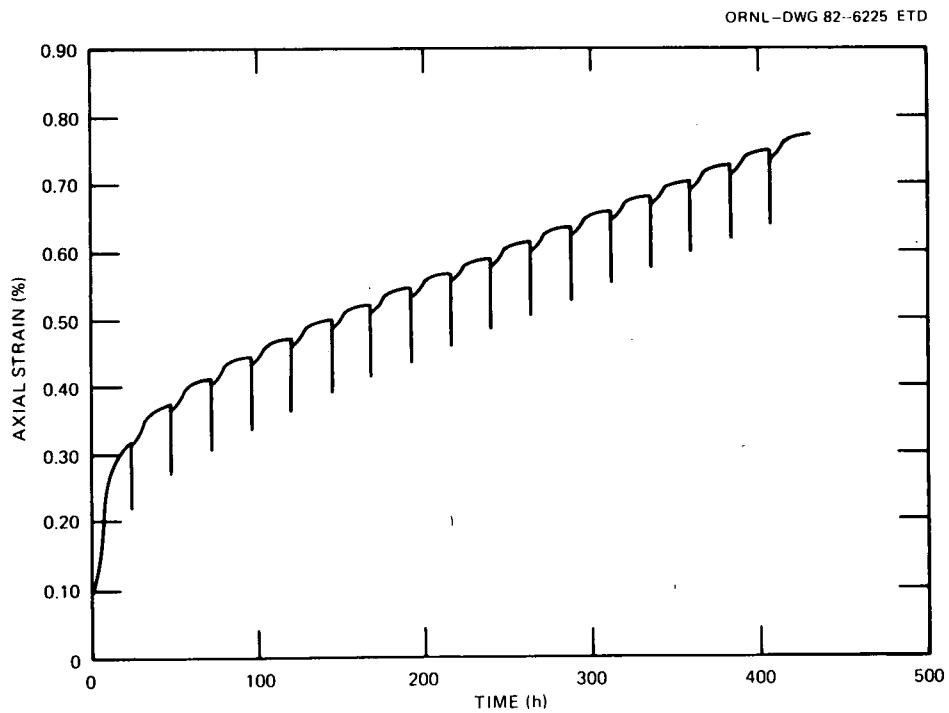


Fig. 10. Predicted axial ratchetting strain vs time for outer element of TT-8 experiment.

Although the hysteretic loops of Figs. 8 and 9 cannot be compared to experimental results, they will be useful for comparing with calculated results obtained using other finite element codes.

4. GENERAL PROPERTIES OF SOLUTIONS USING THE UNIFIED EQUATIONS

Much attention has been paid in this and in past writings to the materials aspects of the unified equations, to their detailed predictions of observed behavior, and to their co-relationship with physical and metallurgical models. However, also important from the standpoint of conducting structural analyses are the continuum aspects of constitutive equations relating to well-posed structural problems and well-behaved stable solutions to these problems. For example, it is of importance to the structural analyst to know how strongly his solution to a given structural problem, based on a given set of constitutive relationships, is influenced by the assumed initial stress and inelastic state fields. Looked at another way, he must know whether the solutions to two structural problems, whose histograms and conditions are identical except for the initial stress and state fields, eventually converge or perhaps even diverge. If the latter is true, he must seriously ask whether the real structure being modeled behaves in that way or whether the constitutive relationships being used are inappropriate. If the structure does behave in that way, there is little hope for detailed structural analysis as a useful tool because it is generally impossible to know the initial stress and inelastic state distribution; indeed, the structure is usually analyzed before it is built. Fortunately, there is evidence that real structures undergoing inelastic deformation, particularly at elevated temperature, do have a fading memory of their initial stress and state, and eventually respond uniquely to a given loading and temperature history. This being the case, it makes sense to require that mathematical models of structural behavior also possess such properties.

In this section, we investigate some of the general properties of solutions of structural problems that can be expected when using the ORNL unified constitutive equations. To that end, an expression relating conditions for two distinct solutions will first be derived. This expression will be used subsequently in demonstrating general properties of solutions.

For small changes in stress at constant state, Eqs. (2.1) through (2.8) satisfy the condition*

$$d\sigma_{ij} d\dot{\epsilon}_{ij} \geq 0 ; \quad \alpha_{ij} = \text{const.} \quad (4.1)$$

Similarly, for small changes in the state at constant stress, those equations satisfy

$$d\alpha_{ij} d\dot{\alpha}_{ij} \leq 0 ; \quad \sigma_{ij} = \text{const.} \quad (4.2)$$

Following analogous arguments to those of Ponter,¹⁵ use is made of Eqs. (4.1) and (4.2) in deriving an expression that links the conditions at two generic points in the state space $(\sigma_{ij}, \alpha_{ij})$. We consider a straight-line path between the two points $(\sigma_{ij}^1, \alpha_{ij}^1)$ and $(\sigma_{ij}^2, \alpha_{ij}^2)$, that is to say, we consider a path for which $(d\sigma_{ij}, d\alpha_{ij})$ has a fixed direction. The monotonic progress of the point $(\sigma_{ij}, \alpha_{ij})$ along the path can be characterized by

$$\sigma_{ij} = \sigma_{ij}^1 + \lambda(\sigma_{ij}^2 - \sigma_{ij}^1) \quad (4.3)$$

and

$$\alpha_{ij} = \alpha_{ij}^1 + \lambda(\alpha_{ij}^2 - \alpha_{ij}^1) , \quad (4.4)$$

where λ increases monotonically from zero to one, i.e.,

$$0 \leq \lambda \leq 1 \text{ and } d\lambda > 0 . \quad (4.5)$$

The differentials $d\sigma_{ij}$ and $d\alpha_{ij}$ at some point on the path are then

$$d\sigma_{ij} = d\lambda(\sigma_{ij}^2 - \sigma_{ij}^1) \quad (4.6)$$

and

$$d\alpha_{ij} = d\lambda(\alpha_{ij}^2 - \alpha_{ij}^1) . \quad (4.7)$$

Multiplying Eq. (4.6) by $d\dot{\epsilon}_{ij}$ and Eq. (4.7) by $d\dot{\alpha}_{ij}$ and making use of

*Equation (4.1) is equivalent to the extended form of Drucker's stability postulate (in the small).

Eqs. (4.1) and (4.2), we get

$$(\sigma_{ij}^2 - \sigma_{ij}^1) d\dot{\epsilon}_{ij} d\lambda \geq 0 \quad (4.8)$$

and

$$(\alpha_{ij}^2 - \alpha_{ij}^1) d\dot{\alpha}_{ij} d\lambda \leq 0 . \quad (4.9)$$

Adding Eqs. (4.8) and (4.9), we have, corresponding to any point along the straight-line path,

$$[(\sigma_{ij}^2 - \sigma_{ij}^1) d\dot{\epsilon}_{ij} - (\alpha_{ij}^2 - \alpha_{ij}^1) d\dot{\alpha}_{ij}] d\lambda \geq 0 . \quad (4.10)$$

Integration along the path then yields

$$(\sigma_{ij}^2 - \sigma_{ij}^1) (\dot{\epsilon}_{ij}^2 - \dot{\epsilon}_{ij}^1) - (\alpha_{ij}^2 - \alpha_{ij}^1) (\dot{\alpha}_{ij}^2 - \dot{\alpha}_{ij}^1) \geq 0 , \quad (4.11)$$

where $\dot{\epsilon}_{ij}^1$ and $\dot{\epsilon}_{ij}^2$ are the inelastic strain rates, and $\dot{\alpha}_{ij}^1$ and $\dot{\alpha}_{ij}^2$ are the rates of change of inelastic state at the respective state points $(\sigma_{ij}^1, \alpha_{ij}^1)$ and $(\sigma_{ij}^2, \alpha_{ij}^2)$. Equation (4.11) relates the pertinent field quantities at two generic points in state space.

Equality in Eq. (4.11) holds when the state points coincide (i.e., when $\sigma_{ij}^2 = \sigma_{ij}^1$ and $\alpha_{ij}^2 = \alpha_{ij}^1$), which, in turn, implies that $\dot{\epsilon}_{ij}^2 = \dot{\epsilon}_{ij}^1$ and $\dot{\alpha}_{ij}^2 = \dot{\alpha}_{ij}^1$. Alternatively, equality holds under the rather special circumstance that $\dot{\alpha}_{ij}^2 = \dot{\alpha}_{ij}^1$ and $\dot{\epsilon}_{ij}^2 = \dot{\epsilon}_{ij}^1 = 0$. Examining Eqs. (2.1) through (2.8), we see that these conditions imply $\alpha_{ij}^2 = \alpha_{ij}^1$, but allow $\sigma_{ij}^2 \neq \sigma_{ij}^1$. The condition $\dot{\epsilon}_{ij}^2 = \dot{\epsilon}_{ij}^1 = 0$ corresponds to *shakedown* which will be further discussed later in this section.

A convenient starting point in this discussion of general properties of solutions is, as discussed earlier, the question of convergence of solutions of structural problems that differ only in their initial conditions. We consider two problems in which the structures are identical and each is subjected to an identical loading and temperature history for time $t > 0$. In one case, the initial stress distribution is given by $\sigma_{ij}^1(x_k, 0)$ and the initial inelastic state distribution is given by $\alpha_{ij}^1(x_k, 0)$. Let the solution of that problem be represented by the stresses $\sigma_{ij}^1(x_k, t)$, the inelastic state field $\alpha_{ij}^1(x_k, t)$, the inelastic

strain rates $\dot{\epsilon}_{ij}^1(x_k, t)$, and the displacement rates $\dot{u}_i^1(x_k, t)$. In the second problem, let the initial stress and state distributions be $\sigma_{ij}^2(x_k, 0)$ and $\alpha_{ij}^2(x_k, 0)$, respectively, and the corresponding solution be denoted by $\sigma_{ij}^2(x_k, t)$, $\alpha_{ij}^2(x_k, t)$, $\dot{\epsilon}_{ij}^2(x_k, t)$, and $\dot{u}_i^2(x_k, t)$.

The difference in the stress fields $(\sigma_{ij}^2 - \sigma_{ij}^1)$ is self equilibrating because each stress field is in equilibrium with the same loads. Furthermore, the differences in the total strain rates $(\dot{\epsilon}_{ij}^2 - \dot{\epsilon}_{ij}^1)$ and the displacements rates $(\dot{u}_i^2 - \dot{u}_i^1)$ are kinematically admissible* since $\dot{\epsilon}_{ij}^1, \dot{u}_i^1$ and $\dot{\epsilon}_{ij}^2, \dot{u}_i^2$ are each kinematically admissible. Here, we take the total strain rate as the sum of the elastic strain rate $\dot{\epsilon}_{ij}^e$, the thermal strain rate $\dot{\delta}_{ij}$, and the inelastic strain rate $\dot{\epsilon}_{ij}$, i.e.,

$$\dot{\epsilon}_{ij} = \dot{\epsilon}_{ij}^e + \dot{\delta}_{ij} + \dot{\epsilon}_{ij} . \quad (4.12)$$

The principle of virtual work then states:

$$\int_V (\sigma_{ij}^2 - \sigma_{ij}^1) (\dot{\epsilon}_{ij}^2 - \dot{\epsilon}_{ij}^1) dV = 0 . \quad (4.13)$$

Making use of Eq. (4.12) in Eq. (4.13), there results

$$\frac{d}{dt} \int_V \frac{1}{2} C_{ijkl} (\sigma_{ij}^2 - \sigma_{ij}^1) (\sigma_{kl}^2 - \sigma_{kl}^1) dV + \int_V (\sigma_{ij}^2 - \sigma_{ij}^1) (\dot{\epsilon}_{ij}^2 - \dot{\epsilon}_{ij}^1) dV = 0 , \quad (4.14)$$

where the C_{ijkl} in the first term are the elastic constants in Hooke's law.† As the temperature histories in the two problems are identical, the thermal strain rates $\dot{\delta}_{ij}$ do not contribute to Eq. (4.14). Combining

*By kinematical admissibility it is meant that the strain rates are compatible, i.e., derivable from the displacement rates, and that the displacement rates satisfy the kinematic boundary conditions.

†Here the elastic constants C_{ijkl} are taken to be functions of temperature. For full isotropy, there are only two independent elastic constants, say E and ν . The reason for retaining the full C_{ijkl} here is not to achieve full generality but only for convenience of notation.

Eqs. (4.14) and (4.11), there results

$$\frac{d}{dt} \int_V \left[\frac{1}{2} C_{ijkl} (\sigma_{ij}^2 - \sigma_{ij}^1) (\sigma_{kl}^2 - \sigma_{kl}^1) + \frac{1}{2} (\alpha_{ij}^2 - \alpha_{ij}^1) (\alpha_{ij}^2 - \alpha_{ij}^1) \right] dV \leq 0 \quad (4.15)$$

Denoting the integral in Eq. (4.15) by I , we write

$$\dot{I} \leq 0 \quad (4.16)$$

The first term in the integral I represents the elastic complementary energy of the stress difference $(\sigma_{ij}^2 - \sigma_{ij}^1)$ and serves as a convenient scalar measure of the stress difference in the two solutions. The second term can be viewed similarly as a measure of the difference in the inelastic states $(\alpha_{ij}^2 - \alpha_{ij}^1)$. Thus I , which is a positive definite quantity and zero only when $\sigma_{ij}^2 = \sigma_{ij}^1$ and $\alpha_{ij}^2 = \alpha_{ij}^1$ everywhere in the structure, provides an integrated measure of the difference in the two solutions. Equation (4.16) states that I can only decrease in time or remain constant, i.e., the solutions cannot diverge under the unified equations.

Equality in Eq. (4.16), i.e., $\dot{I} = 0$, corresponds to equality in Eq. (4.11) being satisfied over the entire volume of the structure. Based on the discussion earlier in this section, this occurs when $\sigma_{ij}^2 = \sigma_{ij}^1$ and $\alpha_{ij}^2 = \alpha_{ij}^1$ everywhere, i.e., the same condition for $I = 0$. This says that $\dot{I} = 0$ only when $I = 0$, or that the two solutions continue to converge until they coincide and remain in coincidence thereafter.

As also indicated earlier, an alternative condition for equality in Eq. (4.11) is $\dot{\alpha}_{ij}^2 = \dot{\alpha}_{ij}^1$ and $\dot{\epsilon}_{ij}^2 = \dot{\epsilon}_{ij}^1 = 0$. Although Eqs. (2.1) through (2.8) permit $\dot{\epsilon}_{ij} = 0$ in certain regions of the state space, it is not generally possible for this to be satisfied throughout the entire volume of a loaded structure.* However, with $\dot{\alpha}_{ij}^2 = \dot{\alpha}_{ij}^1$ and $\dot{\epsilon}_{ij}^2 = \dot{\epsilon}_{ij}^1 = 0$ in

*Equations (2.1) through (2.8) permit $\dot{\epsilon}_{ij} = 0$ only when the effective stress is below the threshold κ , i.e., when $J_2 < \kappa$ ($F < 0$), and at points where partial stress reductions have occurred. Under the latter conditions, $\dot{\epsilon}_{ij} = 0$ only for a finite time.

isolated regions and $\sigma_{ij}^2 = \sigma_{ij}^1$ and $\alpha_{ij}^2 = \alpha_{ij}^1$ elsewhere, we can have equality in Eq. (4.16) and have $\dot{I} = 0$ with $I \neq 0$. In other words, it is hypothetically possible to have convergence of the solutions everywhere except in isolated regions where $\dot{\epsilon}_{ij}^2 = \dot{\epsilon}_{ij}^1 = 0$.* These special circumstances are of no practical importance and therefore will not be discussed further.

Thus, it can be stated generally that *the two solutions, having initially different stress and state conditions, eventually converge in the sense of Eq. (4.16) under the ORNL unified equations.* This affords some comfort to the structural analyst that his assumed, and no doubt erroneous, initial conditions may nevertheless lead to the correct stress and strain fields.

It is of interest at this point to briefly compare some other well-known constitutive relations in the present context. For example, for an elastic perfectly-plastic model Eq. (4.2) is trivially satisfied, or equivalently the second term in Eq. (4.11) vanishes because $\alpha_{ij} \equiv 0$. The remaining term of Eq. (4.11), alternately derivable directly from Drucker's postulate, leads to a development for perfect plasticity similar to that given above for the unified model, showing that solutions to structural problems differing only in their initial stress distribution converge. However, for the perfectly plastic model, this holds true only for continued plastic deformation; under shakedown conditions, the shakedown stress state is generally dependent on the assumed initial stress field.

Going a step further to the linear kinematic hardening plasticity model, we have $\alpha_{ij} \neq 0$. In this case, Eq. (4.2) cannot be shown to be valid, and it appears that no general statement can be made indicating convergence of solutions in the sense considered above. However, it is expected that for the linear kinematic hardening model modified by the α -reset option of NE standard F 9-5T,¹⁰ a statement analogous to Eq. (4.2) can be made and that convergence can be demonstrated. Proof is left to future work.

*This is entirely analogous to the situation in classical plasticity.

Returning to the consideration of the unified equations, we observe that Eqs. (4.15) and (4.16) imply that if the initial conditions in the two identical and identically loaded structures are the same, then both $I = 0$ and $\dot{I} = 0$ for all time, i.e., the solutions always remain identical. In other words, *there is a unique solution, under the unified equations, corresponding to a given set of initial conditions, loading, and temperature histories.* Uniqueness may be an assured property of the real world, but it must be demonstrated in the case of mathematical idealizations of real behavior.

Many important structural problems related to the design of LMFBR components involve cyclic histograms of temperature and loading. For this reason it is of interest to consider in some detail the properties of cyclic solutions when employing the ORNL unified constitutive equations. This can be addressed by interpreting Eqs. (4.11) and (4.16) in a slightly different way. Here, instead of considering two identical structures, we consider only one that is subjected to a periodic loading and temperature history. Calling the period of loading τ , the solutions designated (1) and (2) in Eqs. (4.11) and (4.15) can be identified with conditions at time t and $t + \tau$, respectively. That is to say, $\sigma_{ij}^1 \equiv \sigma_{ij}(x_k, t)$ and $\sigma_{ij}^2 \equiv \sigma_{ij}(x_k, t + \tau)$ and similarly with the inelastic state $\alpha_{ij}^1 \equiv \alpha_{ij}(x_k, t)$ and $\alpha_{ij}^2 \equiv \alpha_{ij}(x_k, t + \tau)$. With this interpretation, all the arguments behind Eq. (4.11) and those leading up to Eq. (4.16) remain valid.

As the structure responds to the cyclic loads, the integral I will decrease, according to Eq. (4.16), whenever equality in Eq. (4.11) is not satisfied at all points in the structure. As the quantity I cannot become negative and thus cannot continue to decrease indefinitely, it is expected that there will be a time, corresponding to the passage of n cycles, that equality in Eq. (4.11) will be satisfied everywhere, i.e., for $t > n\tau$, $\dot{I} = 0$ and I becomes constant.

As in the earlier convergence argument, the only meaningful set of conditions leading to $\dot{I} = 0$ is $\sigma_{ij}^2 = \sigma_{ij}^1$ and $\alpha_{ij}^2 = \alpha_{ij}^1$ everywhere in the structure, corresponding to $I = 0$. Here, this means that $\sigma_{ij}(x_k, t) = \sigma_{ij}(x_k, t + \tau)$ and $\alpha_{ij}(x_k, t) = \alpha_{ij}(x_k, t + \tau)$ for $t > n\tau$. In other words, *the stress and inelastic state fields also become periodic with period τ .*

This further implies that a limit cycle is inevitably reached in the state space $(\sigma_{ij}, \alpha_{ij})$ for $t > n\tau$. Intuitively, it would seem necessary that such a limit cycle be reached after a sufficiently large number of loading cycles.* The predicted response of TT-8, depicted in Figs. 8, 9, and 10, provides a good example of a cyclically loaded structure reaching a state limit cycle (not shown) although the stress-strain response clearly has not.

As indicated earlier, $\sigma_{ij}^2 = \sigma_{ij}^1$ and $\alpha_{ij}^2 = \alpha_{ij}^1$ imply that $\dot{\epsilon}_{ij}^2 = \dot{\epsilon}_{ij}^1$, so that the inelastic strain rate field also becomes periodic. As we are considering the case where generally $\dot{\epsilon}_{ij} \neq 0$, there are continuing inelastic strains for $t > n\tau$, which themselves may become periodic, corresponding to a condition of alternating inelastic deformation, or non-periodic leading to a condition of incremental inelasticity or ratcheting. The former may ultimately lead to a low-cycle fatigue failure in the structure. The latter, exemplified in Figs. 8, 9, and 10, may eventually lead to failure resulting from unbounded deformation.

As noted before, a second set of conditions theoretically satisfying equality in Eq. (4.11) includes $\dot{\epsilon}_{ij}^2 = \dot{\epsilon}_{ij}^1 = 0$, corresponding to shakedown. Also as argued earlier, this condition cannot practically be satisfied everywhere in the structure under the unified equations. Thus, shakedown in the strict sense cannot occur; however, a pseudo-shakedown state can be reached as relatively large, short-term plastic deformations give way to creep deformations under continued loading. More on the subject of shakedown and the extension of classical shakedown theorems relative to the unified equations is presently being investigated and will be the subject of a future report.

A special case of the periodic loading is that of constant external loads and a constant temperature distribution. In this case, the stress and inelastic state fields eventually become constant in time. With $\dot{\alpha}_{ij}$ and the elastic strain rate $\dot{\epsilon}_{ij}^e$ everywhere equal to zero, the total

*This is not generally the case if the inelastic strain itself is included as a state variable, which is effectively the case for linear kinematic hardening plasticity.

strain rate is, according to Eqs. (2.1) through (2.8),

$$2\mu\dot{\epsilon}_{ij} = \left(\frac{r}{h}\right) \frac{\alpha_{ij}}{\sqrt{I_2}}, \quad (4.17)$$

and depends only on the inelastic state α_{ij} . Moreover, at steady state, the stresses σ_{ij} (or deviatoric stress S_{ij}) and α_{ij} are also directly related through Eq. (2.1) so that the response is equivalent to nonlinear viscous behavior.

5. SUMMARY AND CONCLUSIONS

A multiaxial, nonisothermal statement of the ORNL unified constitutive equations has been presented with material parameters specified for a VAR heat (heat 56448) of 2-1/4 Cr-1 Mo steel in a 40-h PWHT condition. This heat and condition were selected as being prototypical of LMFBR steam generator material and conditions. Specific results of characterization testing have not been included nor has a detailed description of the procedure through which the model parameters were determined from the test results. These topics have been covered in previous publications.^{1,2,12,16}

The unified equations have already been implemented into the ORNL finite element code PLACRE and exercised to a limited degree. It is anticipated that with the publication of this report, the unified equations may find their way into some of the larger, user-oriented codes such as MARC or ABAQUS. Only then can the equations be realistically exercised and a meaningful assessment be made regarding their eventual adoption in NE standard F 9-5T.¹⁰

A number of calculated results using the unified constitutive equations have been given ranging from predictions of simple uniaxial behavior to the complex multiaxial, nonisothermal response of a cylinder (pipe) under thermal transient conditions. It is recommended that several of these results be reproduced to verify correct implementation of the unified model into a given analysis code.

A conspicuous omission in this report is that of multiaxial test results in support of the multiaxial concepts embedded in the ORNL unified theory. Quality high-temperature, multiaxial experiments involving statically determinate stress states and independently measured strains are in desperate need for assessing, not only the unified equations, but any multiaxial formulation, including the F 9-5T¹⁰ constitutive equations. With the recent development of a precision, high-temperature, multiaxial extensometer at ORNL,¹⁷ such experiments are just now getting under way. Results of these experiments will be presented in a subsequent report. Preliminary analysis of some biaxial results show favorable support of the ORNL unified model.

Also discussed in this report are general properties of solutions to structural problems when using the ORNL unified constitutive equations. Conclusions drawn from that study may be summarized as follows.

- The stress and inelastic state fields corresponding to a given loading and temperature history eventually become independent of the initial conditions of stress and inelastic state (fading memory).
- The stress and inelastic state fields are unique for given initial conditions and a given loading and temperature history.
- Periodic loading and temperature histories eventually lead to periodic stress and inelastic state fields. A limit cycle in the state space is assured.
- Constant loading and temperature eventually lead to a steady-state response equivalent to nonlinear viscous behavior.

ACKNOWLEDGMENTS

The authors wish to thank W. K. Sartory for his substantive contribution in numerically implementing the unified equations in PLACRE, conducting most of the analyses, and reviewing the manuscript. Thanks also go to J. R. Ellis for his helpful discussions concerning this work, his careful development and experimental work, and his part in reviewing the manuscript. Thanks to J. M. Corum for supporting this work in the High-Temperature Structural Design Technology program and, finally, thanks to M. W. Teague for the final typing of this manuscript.

REFERENCES

1. R. W. Swindeman and D. N. Robinson, *Experimental Methods to Determine the Kinematic State Variable in 2-1/4 Cr-1 Mo Steel at High Temperature*, ORNL-5776 (July 1981).
2. R. W. Swindeman and B. C. Williams, *Evaluation of the Mechanical Behavior of VAR 2-1/4 Cr-1 Mo Steel in Support of Constitutive Equation Development*, ORNL/TM-8402 (to be published).
3. D. N. Robinson, *A Unified Creep-Plasticity Model for Structural Metals at High Temperature*, ORNL/TM-5969 (November 1978).
4. J. R. Rice, "On the Structure of Stress-Strain Relations for Time-Dependent Plastic Deformations in Metals," *J. Appl. Mech., Trans. ASME* 37, Series E, No. 3, 728-37 (September 1970).
5. A.R.S. Ponter and F. A. Leckie, "Constitutive Relationships for the Time-Dependent Deformation of Metals," *J. Eng. Mater. Technol., Trans. ASME* 98, 47-51 (1976).
6. S. K. Mitra and D. McLean, "Work Hardening and Recovery in Creep," *Proc. Roy. Soc. (London)* 295(a), 288-99 (1961).
7. R. Lagneborg, "A Modified Recovery-Creep Model and Its Evaluation," *Met. Sci. J.* 6, 127-33 (1972).
8. E. T. Onat, *Representation of Inelastic Behavior*, ORNL/Sub-3863/2 (November 1976).
9. R. W. Swindeman et al., *Two-Bar Thermal Ratchetting Experiments on 2-1/4 Cr-1 Mo Steel*, ORNL/TM-8001 (January 1982).
10. *Guidelines and Procedures for Design of Class 1 Elevated Temperature Nuclear System Components*, NE Standard F 9-5T, U.S. Department of Energy (March 1981).
11. L. E. Malvern, *Introduction to the Mechanics of a Continuous Medium*, Prentice-Hall, Englewood Cliffs, N.J., 1969.
12. D. N. Robinson, "Development of Advanced Constitutive Laws," *High-Temperature Structural Design Program Prog. Rep. Dec. 31, 1980*, ORNL-5737, pp. 12-19.
13. W. K. Sartory, "Analysis of the ORNL Two-Bar Ratchetting Test SBRI," *High-Temperature Structural Design Program Prog. Rep. June 30, 1980*, ORNL-5683, pp. 9-13.
14. *Nuclear Systems Materials Handbook, Vol. 1: Design Data*, TID-26666, Hanford Engineering Development Laboratory.

15. A.R.S. Ponter, "Convexity and Associated Continuum Properties of a Class of Constitutive Relationships," *J. de Mécanique* 15(4), 527-42 (1976).
16. D. N. Robinson, "Development of a Unified Constitutive Model," *High-Temperature Structural Design Program Prog. Rep. June 30, 1981*, ORNL-5794, pp. 19-22.
17. J. R. Ellis, "Design and Development of a High-Temperature Multiaxial Extensometer," *High-Temperature Structural Design Program Prog. Rep. June 30, 1981*, ORNL-5794, pp. 24-35.

ORNL/TM-8444
Dist. Category UC-79T,
-79Th, -79Tk

Internal Distribution

- | | |
|----------------------|--------------------------------------|
| 1. R. L. Battiste | 17. S. E. Moore |
| 2. J. J. Blass | 18. C. E. Pugh |
| 3. C. R. Brinkman | 19-23. D. N. Robinson |
| 4. S. J. Chang | 24. W. K. Sartory |
| 5. J. A. Clinard | 25-29. R. W. Swindeman |
| 6. J. M. Corum | 30. M. W. Teague |
| 7. J. R. Ellis | 31. H. E. Trammell |
| 8. U. Gat | 32. D. B. Trauger |
| 9. W. L. Greenstreet | 33. G. D. Whitman |
| 10. D. S. Griffith | 34. G. T. Yahr |
| 11. R. C. Gwaltney | 35. Patent Office |
| 12. W. O. Harms | 36. Central Research Library |
| 13. R. L. Huddleston | 37. Document Reference Section |
| 14. Y. L. Lin | 38-39. Laboratory Records Department |
| 15. K. C. Liu | 40. Laboratory Records (RC) |
| 16. W. J. McAfee | |

External Distribution

- 41-42. Director, Office of Breeder Technology Projects, Department of Energy, Washington, D.C. 20545
43. Office of Assistant Manager for Energy Research and Development, DOE, ORO, Oak Ridge, TN 37830
44. Director, Nuclear Research and Development Division, DOE, ORO, Oak Ridge, TN 37830
- 45-183. Given distribution as shown in DOE/TIC-4500 under categories UC-79T (Liquid Metal Fast Breeder Reactors); UC-79Th (LMFBR - Structural Materials and Design Engineering); UC-79Tk (LMFBR - Components)